frontiers in Immunology

ORIGINAL RESEARCH
published: 21 October 2021
doi: 10.3389/fimmu.2021.750229

Pathology and Immunity After SARS-CoV-2 Infection in Male Ferrets Is Affected by Age and Inoculation Route

*Koen van de Ven[1], Harry van Dijken[1], Lisa Wijsman[1], Angéla Gomersbach[2], Tanja Schouten[2], Jolanda Kool[1], Stefanie Lenz[1], Paul Roholl[3], Adam Meijer[1], Puck B. van Kasteren[1] and Jørgen de Jonge[1]**

[1] Centre for Infectious Disease Control, National Institute for Public Health and The Environment (RIVM), Bilthoven, Netherlands, [2] Animal Research Centre, Poonawalla Science Park, Bilthoven, Netherlands, [3] Microscope Consultancy, Weesp, Netherlands

OPEN ACCESS

Edited by:
Yasushi Itoh, Shiga University of Medical Science, Japan

Reviewed by:
Vladimír Jekl, University of Veterinary and Pharmaceutical Sciences Brno, Czechia
Morgane Bomsel, Centre National de la Recherche Scientifique (CNRS), France

***Correspondence:**
Jørgen de Jonge
jorgen.de.jonge@rivm.nl

Specialty section:
This article was submitted to Viral Immunology, a section of the journal Frontiers in Immunology

Received: *30 July 2021*
Accepted: *04 October 2021*
Published: *21 October 2021*

Citation:
van de Ven K, van Dijken H, Wijsman L, Gomersbach A, Schouten T, Kool J, Lenz S, Roholl P, Meijer A, van Kasteren PB and de Jonge J (2021) Pathology and Immunity After SARS-CoV-2 Infection in Male Ferrets Is Affected by Age and Inoculation Route. Front. Immunol. 12:750229. doi: 10.3389/fimmu.2021.750229

Improving COVID-19 intervention strategies partly relies on animal models to study SARS-CoV-2 disease and immunity. In our pursuit to establish a model for severe COVID-19, we inoculated young and adult male ferrets intranasally or intratracheally with SARS-CoV-2. Intranasal inoculation established an infection in all ferrets, with viral dissemination into the brain and gut. Upon intratracheal inoculation only adult ferrets became infected. However, neither inoculation route induced observable COVID-19 symptoms. Despite this, a persistent inflammation in the nasal turbinates was prominent in especially young ferrets and follicular hyperplasia in the bronchi developed 21 days post infection. These effects -if sustained- might resemble long-COVID. Respiratory and systemic cellular responses and antibody responses were induced only in animals with an established infection. We conclude that intranasally-infected ferrets resemble asymptomatic COVID-19 and possibly aspects of long-COVID. Combined with the increasing portfolio to measure adaptive immunity, ferrets are a relevant model for SARS-CoV-2 vaccine research.

Keywords: SARS-CoV-2, cellular immunity, humoral immunity, animal models, pathology, COVID-19

INTRODUCTION

Severe acute respiratory syndrome coronavirus 2 (SARS-CoV-2) was first detected in patients near the end of 2019 and soon started a new pandemic (1). As an intervention, effective SARS-CoV-2 vaccines were rapidly developed and implemented. Although many of these vaccines have proven to be effective in limiting mortality and morbidity (2), it remains a point of concern that SARS-CoV-2 mutants might escape vaccine-induced immunity (3). Additionally, much remains unknown about the pathology and long-term effects of SARS-CoV-2 infection and protective immunity. Animal models are essential for investigating these issues and the scientific community has made unprecedented advances in their development since the outbreak (4, 5). However, there are still some remaining knowledge gaps that limit the evaluation of outstanding questions.

SARS-CoV-2 spreads through direct contact, aerosols, or droplets (6–9). Viral RNA has been detected in stool samples of infected individuals (10–12) and this has raised the question whether

the fecal-oral route could also facilitate SARS-CoV-2 transmission (13). The virus primarily replicates in respiratory tissue, but viral RNA has been detected in many other tissues including the brain, gut, heart, and endothelial lining of the vascular system (12, 14, 15). SARS-CoV-2 infection usually induces mild disease (COVID-19), with symptoms limited to fever, dry cough, anosmia/ageusia, myalgia, fatigue, dyspnea, sputum production, headache, and occasionally diarrhea [reviewed in (16)]. Fatal cases are marked by respiratory failure, arrhythmia, shock, and acute respiratory distress syndrome (15, 17, 18). Mortality significantly increases with age and certain comorbidities such as cardiovascular disease and diabetes (15, 17, 19–21). Despite similar infection rates between men and women, men are more likely to succumb to infection (17, 19, 20). Some individuals additionally suffer from 'long-COVID' (post-acute COVID-19 syndrome) where they experience persisting symptoms long after initial SARS-CoV-2 infection (22).

As the ferret (*Mustela putorius furo*) is considered the best small animal model for respiratory disease caused by influenza virus (23, 24), multiple groups have investigated if ferrets are also suited to model COVID-19 (25–33). From these studies, we know that SARS-CoV-2 efficiently replicates in the upper respiratory tract (URT) of ferrets upon intranasal (i.n.) inoculation, but replication in the lower respiratory tract (LRT) is limited (25). There are however still many unknowns regarding the ferret model.

Here, we report our efforts to investigate the influence of both age and inoculation route on SARS-CoV-2 infection in the ferret model. As intratracheal (i.t.) inoculation with influenza virus induces more severe disease in ferrets (34–36), we wondered if we could model severe COVID-19 in ferrets by i.t. inoculation with SARS-CoV-2. In addition, as advancing age is a risk factor for the development of severe disease (17, 19, 20), we investigated the role of age by infecting both young and adult ferrets. We found that SARS-CoV-2 infection was more efficient *via* the i.n. route and that i.t. inoculation and increased age did not result in more severe disease. Regardless of age and inoculation route, no clinical disease was observed. Despite the absence of symptoms, we did find pathological aberrations in the nasal turbinates and lungs that were more prominent in young ferrets and seemed to increase with time, potentially reflecting long-COVID in humans. We also report that humoral and cellular immune responses appear to depend on sufficient viral load during the acute phase of the infection. Together, our findings indicate that while ferrets might not be suited to study severe COVID-19, they can be used to model viral replication, adaptive immune responses, asymptomatic COVID-19 and possibly long-COVID.

MATERIALS & METHODS

Ethical Statement

All animal experiments were conducted in line with EU legislation. The experiment was approved by the Animal Welfare Body of the Antonie van Leeuwenhoek terrain (Bilthoven, The Netherlands) under permit number AVD3260020184765 of the Dutch Central Committee for Animal experiments. Ferrets received food and water ad libitum and were inspected daily. If ferrets reached the pre-defined end points, they would be euthanized by cardiac bleeding under anesthesia with ketamine (5 mg/kg; Alfasan) and medetomidine (0.1 mg/kg; Orion Pharma). Endpoints were scored based on clinical parameters for activity (0 = active; 1 = active when stimulated; 2 = inactive and 3 = lethargic) and impaired breathing (0 = normal; 1 = fast breathing; 2 = heavy/stomach breathing). Ferrets were euthanized when they reached score 3 on activity level (lethargic) or when the combined score of activity and impaired breathing reached 4.

Cell and Virus Culture

VERO E6 cells were cultured in DMEM (Gibco; Thermo Fisher Scientific) supplemented with 1x penicillin-streptomycin-glutamine (Gibco) and 10% fetal bovine serum (FBS; HyClone, GE Healthcare). SARS-CoV-2 virus was originally isolated from a Dutch patient (hCoV-19/Netherlands/ZuidHolland_10004/2020) and grown on VERO E6 cells in infection medium consisting of DMEM, 1x penicillin-streptomycin-glutamine and either 0% or 2% FBS. When >90% cytopathic effect (CPE) was observed, the suspension was spun down for 10 minutes at 4000x g to pellet cell debris. The remaining suspension was aliquoted and stored at -80°C. Sequencing of virus stock used for infection revealed that no mutations had occurred compared to the primary isolate (GISAID accession ID: EPI_ISL_454753) and that the furin cleavage site was maintained. Wild-type mumps virus (MuVi/Utrecht.NLD/40.10; genotype G) was grown on Vero cells in DMEM (Gibco) with 2% FBS. Upon >90% CPE, the supernatant of the infected Vero cells was centrifuged at 500x g, filtered (5um pore size) and aliquots were stored at -80°C.

Animal Handling

Young (9-10 months) and adult (36-48 months) outbred male ferrets (Schimmel b.v., The Netherlands) arrived at the animal research facility (ARC, Bilthoven, The Netherlands) at least one week before commencement of the study. From arrival till the day of infection, ferrets were housed in open cages per group. Animals with confirmed exposure to Aleutian disease or NL63 were housed in a separate chamber. Infections were carried out in BSL-3 classified isolators where the ferrets remained till the end of the experiment. Placement of temperature transponders and infections were carried out under anesthesia with ketamine (5 mg/kg) and medetomidine (0.1 mg/kg). Buprenodale (0.2ml; AST Farma) was administered after transponder placement as a post-operative analgesic. Anesthesia was antagonized with atipamezole (0.25 mg/kg; Orion Pharma), which was delayed by 30 minutes in case of infections to prevent secretion of the inoculum by sneezing or coughing. Weight determinations and swabbing occurred under anesthesia with ketamine alone.

Study Design

The study was split into three experiments (A, B and C) that were infected separately with SARS-CoV-2. Ferrets in the A, B and C experiments were respectively dissected 5, 14 and 21 days after infection. Each experiment consisted of 4-5 groups with 3 ferrets each. Groups were defined by their age (young vs adult) and

infection route (intra nasal vs intra tracheal). Due to a shortage of adult ferrets, experiment B did not contain a group with i.n. infected adult ferrets. An additional mock-infected group to control for immunological assays and pathology was added to experiments B (young ferrets) and C (adult ferrets).

On day 0, ferrets were infected i.t. or i.n. with 10^7 $TCID_{50}$ SARS-CoV-2 diluted in PBS. Mock-infected ferrets received PBS i.n. alone. Virus was administered in 0.1ml for i.n. and 3ml for i.t administration. Prior to infection and on every-other day starting from day 3, bodyweight was measured and nasal, throat and rectal swabs were collected. At the end of the experiment, animals were euthanized by bleeding *via* heart puncture under anesthesia with ketamine and medetomidine. Prior to heart puncture, bodyweight was measured and swabs were taken.

Importantly, this study had several complicating factors. At the supplier, males were housed in groups of 3 animals. Due to strict hierarchy present in male ferret groups, we were unable to randomly allocate individual animals to treatment groups. Instead, whole cages (with 3 animals) were randomly allocated to a certain treatment. Before arrival at the animal facility, ferret sera were screened by the European Veterinary Laboratory (EVL, The Netherlands) for prior infections with Aleutian disease, human corona NL63, canine distemper virus (CDV), feline corona virus (FCoV) and canine enteric corona virus (CCoV). FCoV and CCoV are representative for systemic and enteric ferret corona viruses respectively. Almost all animals displayed prior exposure against CDV and multiple animals tested positive for antibodies against NL63, FCoV, CCoV, influenza and Aleutian disease before start of the experiment (**Supplementary Table 1**). Ferrets that tested positive for antibodies against influenza or Aleutian disease were allocated to placebo groups.

Sample Collection

During the experiment, blood was collected from the cranial vena cava and stored in either sodium-heparin coated VACUETTE tubes (Greiner) for cellular assays or in CAT serum separator clot activator VACUETTE tubes (Greiner) to isolate serum. Blood was kept at RT and analyzed the same day. At the end of the experiment, blood was collected by heart puncture after which groups B and C received a lung perfusion to remove the majority of lymphocytes in the circulation that might affect cellular assays. The lower 4cm of the trachea was stored in formalin to study pathology while the middle 1.5cm was used to determine viral load. Lungs were weighed and the left cranial lobe was inflated with formalin and stored in 10% buffered formalin for histopathological analysis. To assess viral RNA and $TCID_{50}$-titers, 0.5cm slices of the right cranial, middle and caudal lobe were collected in Lysing Matrix A tubes (MP Biomedicals, Germany). Samples in Lysing Matrix A tubes were stored at -80°C until analysis. The rest of the lungs were used for immunological analysis and were kept cold (4°C) o/n until processing the next day.

Of the intestine, 1.5cm parts of the ileum and upper colon were collected in Lysing Matrix A tubes and formalin to assess viral RNA and pathology respectively. Next, the cranium was bisected with an oscillating blade moving from the caudal to the rostral position to prevent contamination of brain tissue by any particles from URT. The nasal turbinates on the left of the septum were used for pathology while the right side was used for virology and immunology. Finally, the olfactory bulb (OB) and sections of the cerebrum and cerebellum were collected for virology and pathology. Samples for pathology, virology and immunology were stored respectively in formalin, Lysing Matrix A tubes and RPMI1640 supplemented with 1x penicillin-streptomycin-glutamine.

Nasal and throat swabs were collected in 2ml transport buffer consisting of 15% sucrose (Merck), 2.5µg/ml Amphotericin B, 100 U/ml penicillin, 100µg/ml streptomycin and 250µg/ml gentamicin (all from Sigma). Rectal swabs were stored in 1ml S.T.A.R. buffer (Roche). After collection, all swabs were vortexed, aliquoted under BSL-3 conditions and stored at -80°C until further analysis. Of each sample, 200µl was directly added to MagNA Pure External Lysis Buffer (Hoffmann-La Roche, Basel, Switzerland), vortexed and stored at -20°C for RT-qPCR. Samples stored in Matrix A tubes were thawed and 750µl of DMEM infection medium (DMEM containing 2% FBS and 1x penicillin-streptomycin-glutamine) was added. Tissues were then dissociated in a FastPrep-24™ by shaking twice for 1 minute after which the samples were spun down for 5 minutes at 4000x g. Of the supernatant, 200µl was used for RT-qPCR analysis as detailed above and 250µl was used for $TCID_{50}$-determination.

The dissection of SARS-CoV-2 infected animals occurred under BSL-3 conditions and all materials from swabs, samples in Lysing Matrix A tubes and nasal turbinates were handled under BSL-3 conditions. Blood was handled under BSL-2 conditions as blood was shown to be PCR-negative for SARS-Cov-2. Spleen and lung dissected 14 and 21 dpi were processed under BSL-2+ conditions as lung tissue did not contain infectious virus 5 d.p.i. as shown by $TCID_{50}$ analysis.

Temperature Logging

In experiments B and C, animals received temperature probes (Star Oddi, Iceland) two weeks before the infection. These probes recorded temperature every 30 minutes from 7 days before infection till the end of the experiment. Fever was calculated as deviation from baseline (ΔT), where the baseline refers to the mean temperature over 5 days prior to SARS-CoV-2 infection.

Pathology

Pathology scoring was performed as described before (16, 28). After fixation, the lung lobes were embedded in paraffin and sliced into 5µm thick sections. Slides were stained with haematoxylin and eosin and microscopically examined at 50x or 100x magnification. For each tissue, at least 20 microscopic fields were scored. Pathological scoring distinguished between the categories 'epithelial damage' and 'inflammation'. Damage related parameters included hypertrophy, hyperplasia, flattened or pseudo squamous epithelia, necrosis and denudation of bronchi (oli) epithelium, hyperemia of septa and alveolar emphysema and haemorrhages. Inflammation related parameters included (peri) bronchi(oli)tis, interstitial infiltrate, alveolitis and (peri)vasculitis characterized by polymorphonuclear (PMN) cells, macrophages

and lymphocytic infiltrate. Pathological findings were scored on a scale of 0 (no aberrations) to 5 (severe damage) and were summarized in two 'end scores' for the categories 'epithelial damage' and 'inflammation'. Microscopic slides were randomized and scored blindly by an experienced pathologist.

Lymphocyte Isolation

Blood collected in sodium-heparin tubes was diluted 1:1 with PBS (Gibco) and layered on top of a 1:1 mixture of Lymphoprep (1.077 g/ml, Stemcell) and Lymphoyte-M (1.0875 g/ml, Cedarlane). The gradient was spun at 800x g for 30 minutes and the interface containing PBMCs was collected. The cells were subsequently washed twice with washing medium (RPMI1640 + 1% FBS) and spun down at 500x g for 10 minutes (first wash) or 5 minutes (second wash). After the final washing step, cells were resuspended in stimulation medium (RPMI1640 + 10% FBS + 1x penicillin-streptomycin-glutamine).

On days 14 and 21 after infection, the lungs of euthanized animals were perfused with saline to remove circulating lymphocytes from the lungs as described before (37). Lymphocytes from the lung were isolated using enzymatic digestion. Lungs were first processed into small dices of approximately $5mm^3$ using scissors. The diced tissue was then digested for 60 minutes at 37°C in 12ml of a pre-heated suspension of collagenase I (2.4mg/ml, Merck) and DNase I (1mg/ml, Novus Biologicals) in RPMI1640 while rotating. Tissue was further homogenized by gently pressing the tissue over a sieve using the plunger of a 10ml syringe. The resulting suspension was diluted with EDTA-supplemented washing medium [RPMI1640 + 1% FBS + 2mM EDTA (Invitrogen)] and filtered over a 70µm cell strainer. This suspension was layered on top of 15ml Lympholyte-M in a 50ml tube. Density centrifugation and washing steps were performed as described above, with the exception that washing medium was supplemented with EDTA to prevent agglutination of cells

SARS-CoV-2 Peptide Pools

PepMix™ peptide pools for T cell stimulation assays were obtained from JPT Peptide Technologies GmbH. Each pool contained 15 amino acids long peptides with an overlap of 11 amino acids spanning an entire protein of SARS-CoV-2. Due to the length of the spike protein, the spike PepMix™ was distributed over two separate vials containing peptides 1-158 and 159-315.

Elispot

Pre-coated Ferret IFNγ-ELISpot (ALP) plates (Mabtech) were used according to the manufacturers protocol. Per well, 250K PBMCs or 31.25K lung lymphocytes were stimulated with live virus (MOI 1) or SARS-CoV-2 peptide pools (1µg/peptide/ml) in ELISpot plates for 20 hours at 37°C. Plates were then washed and developed according to the manufacturers protocol, with the modification that incubation with the first antibody occurred o/n at 4°C instead of 2 hours at RT. After the final washing step, plates were left to dry for >2 days. Plates were then packaged under BSL-3 conditions and heated to 65°C for 3 hours to inactivate any remaining SARS-CoV-2 particles. Plates were analyzed on the ImmunoSpot® S6 CORE (CTL, Cleveland, OH). Spot counts were corrected for background signals by subtracting the number of spots in the medium condition from all other conditions. Data were visualized on a log-scale, so the minimum spot count was set to '1' for visualization purposes.

Trucount

Of each animal, 50µl of heparin-blood was used for trucount analysis with the non-centrifugation PerFix-NC kit (Beckman Coulter). Cells were first stained extracellular with α-CD4-APC (02, Sino Biological), α-CD8a-eFluor450 (OKT8, eBioscience), and α-CD14-PE (Tük4; Thermo Fisher) for 15 minutes at RT. Cells were then fixated with 5µl Fixative Reagent for 15 minutes after which 300µl Permeabilizing reagent was added. The subsequent intracellular staining consisted of α-CD3e-FITC (CD3-12, Biorad) and α-CD79a-APC/eFluor780 (eBioscience). After 15 minutes incubation at RT, 3ml of Final reagent was added to each sample. To decrease measurement time, samples were spun down for 5 minutes at 500x g and 2.8ml suspension was removed. The pellet was resuspended in the remaining volume and 50µl of Precision Count beads (Biolegend) was added to each sample to calculate the absolute number of cells. Samples were measured on a FACSymphony A3 (BD) and analysed using FlowJo™ Software V10.6.2 (BD). An example of the gating strategy is present in **Supplemental Figure 1**.

Virus Titer Analysis

Virus stocks were titrated in octuplicate on VERO E6 cells in 96-wells plates. Samples were titrated in DMEM medium containing 2% FBS and 1x penicillin-streptomycin-glutamine. After 6 days, CPE was scored and $TCID_{50}$ values were calculated using the Reed & Muench method. Nose and throat swabs were similarly tested, but in sextuplicate with 8 dilutions. For swabs, 2.5µg/ml Amphotericin B and 250µg/ml gentamicin was added to the titration medium.

RT-qPCR

Lysis buffer was spiked with equine arteritis virus (EAV) as an internal RT-qPCR control and stored at -20°C until sample material was added. Total nucleic acid was extracted from samples with the MagNA Pure 96 system using the MagNA Pure 96 DNA and Viral NA Small Volume Kit and eluted in a volume of 50µl Roche Tris-HCl elution buffer. A 20µl Real-time Reverse-Transcription PCR (RT-qPCR) reaction contained 5µl of sample nucleic acid, 7µl of 4x Taqman Fast Virus Master Mix (Thermo Fisher), 5µl of DNAse/RNAse free water and 3µl of primers and probe mix (sequences shown in **Table 1**). The in-house SARS-CoV-2 detection assay was performed using E-gene primers and probe specific for SARS-related betacoronaviruses as described by Corman et al. (39) and the equine arteritis virus (EAV) internal control primers and probe as described by Scheltinga et al. (40). This E-gene RT-qPCR detects genomic and subgenomic SARS-CoV-2 RNA molecules. The in-house subgenomic mRNA E-gene assay was performed using the E-gene reverse primer and probe and the forward primer as described by Zhang et al. (41). All tests were performed on a Light Cycler 480 I (LC480 I, Roche) according to the cycling

TABLE 1 | Primers and probes used in this study.

Oligonucleotide	Sequence	Type	Annealing Temperature	Label
E_Sarbeco_F	ACAGGTACGTTAATAGTTAATAGCGT	forward	60°C	
E_Sarbeco_R	ATATTGCAGCAGTACGCACACA	reverse	60°C	
E_Sarbeco_P1	ACACTAGCCATCCTTACTGCGCTTCG	probe	60°C	FAM-BHQ1
EAV-2043F	CTGTCGCTTGTGCTCAATTTAC	forward	60°C	
EAV-2193R	AGCGTCCGAAGCATCTC	reverse	60°C	
EAV 2102P-2	TGCAGCTTATGTTCCTTGCACTGTGTTC	probe	60°C	TXR-BHQ2
Leader_Sars2	CCCAGGTAACAAACCAACCAAC	forward	60°C	
Cyclophilin_A_F	GGTGGTAAGTCCATCTACGG	forward	54°C	
Cyclophilin_A_R	ACTCTGAGATCCAGCTAGGC	reverse	54°C	
ACE2_F	TTGTATCTGTTGGCCTTCCC	forward	53°C	
ACE2_R	TCTTGATCCTGAAGTCACGC	reverse	53°C	
TMPRSS2_F	TGGGTTGAGTCAAATCTGCC	forward	55°C	
TMPRSS2_R	CTACAGTTTACCTGCTGGCC	reverse	55°C	
Beta-actin_F	TGACCGGATGCAGAAGGA (38)	forward	51°C	
Beta-actin_R	CCGATCCACACCGAGTACTT (38)	reverse	51°C	

protocol detailed in **Table 2**. Cycle threshold (Ct) values were recorded.

Total nucleic acid extracted with the MagNA Pure 96 system was used to determine ACE2 and TMPRSS2 expression in a separate reaction. First, cDNA was synthesized from the isolated RNA with the iScript™ cDNA synthesis kit (Bio-Rad) according to the manufacturers protocol using a StepOnePlus RT-PCR system (Thermo Fisher). RT-qPCR was performed using 1x Maxima SYBR Green/ROX qPCR Master Mix (Thermo Fisher) on the StepOnePlus with primers for Cyclophilin A, ACE2, TMPRSS2 and Beta-actin (Isogen Life Science, Netherlands; **Table 1**). RT-qPCR was performed for 10 minutes at 95°C, followed by 40 cycles of 95°C for 30 seconds and primer-specific annealing temperatures (see above) for 45 seconds. This was followed by 95°C for 15 seconds, 53°C for 60 seconds and 95°C for 15 seconds. A pooled reference sample consisting of 5-fold dilutions of cDNA of the nasal turbinates of 6 animals was taken along in duplicate with each RT-qPCR to create a standard curve. RNA concentrations (in arbitrary units) of test samples were interpolated from the standard curve. The relative mRNA expression of target genes ACE2 and TMPRSS2 was calculated by dividing the interpolated arbitrary RNA unit of the target genes by the geometric mean of the endogenous control genes (Cyclophilin A and Beta-actin).

ELISA

Immulon 2 HB 96-well plates (Thermo Fisher) were coated overnight at RT with 100µl/well 0.25µg/ml recombinant SARS-CoV-2 Spike or Spike receptor binding domain protein (Sino biological, China) and washed thrice with PBS + 0.1% Tween-80 before use. Sera were first diluted 1:100 in PBS + 0.1% Tween-80 and then 2-fold serially diluted. Per well, 100µl of diluted sera was added and plates were incubated for 60 minutes at 37°C. After washing thrice with 0.1% Tween-80, plates were incubated for 60 minutes at 37°C with HRP-conjugated goat anti-ferret IgG (Alpha Diagnostic), diluted 1:5000 in PBS containing 0.1% Tween-80 and 0.5% Protivar (Nutricia). Plates were then washed trice with PBS + 0.1% Tween-80 and once with PBS, followed by development with 100µl SureBlue™ TMB (KPL) substrate. Development was stopped after 10 minutes by addition of 100µl 2M H_2SO_4 and OD_{450}-values were determined on the EL808 absorbance reader (Bio-Tek Instruments). Individual curves were visualized using local polynomial regression fitting with R software (42). Antibody titers were determined as the dilution at which antibody responses dropped below background. This background was calculated as the 'mean + 3 * standard deviation' of the OD_{450} at a 400x serum-dilution of all animals tested before SARS-CoV-2 infection.

Data Analysis & Statistics

All raw data was analyzed with the software detailed above. These data were then exported to Excel and loaded into R software (42). Data analysis and visualization of data was carried out using the R packages ggplot2 (43), tidyverse (44) and ggpubr (45). Due to the exploratory goal and small group numbers of this study, statistical analysis was limited. For most assays, groups consisted of 3 ferrets, which we deemed

TABLE 2 | Cycling and temperature protocol for SARS-CoV-2 E-gene RT-qPCR.

PCR Program	Segment number	Temp Target (°C)	Hold Time (sec.)	Slope (°C/sec.)	Acquisition mode	
Reverse Transcription	1	50	900	EXTERNAL*		
Denaturation/Inactivation	1	95	120	EXTERNAL*		
Denaturation	1	95	60	4.4	None	LC480
Amplification	1	95	10	4.4	None	LC480
(cycles:50)	2	60	30	2.2	Single	LC480
Cooling	1	40	30	4.4	None	LC480

**cDNA was synthesized on a thermal block after which the reactions were transferred to the LC480 thermal cycler.*

insufficient for statistical testing. In case of blood cell counts, groups could be combined into young and adult animals. These groups were sufficiently large for statistical comparison, which was performed in R using the Wilcoxon signed-rank test and a correction for multiple testing by the Holm-Bonferroni method (46).

RESULTS

Study Outline

In this study we assessed the role of age and infection route on SARS-CoV-2 disease and immunity in ferrets, in an attempt to model the (severe) COVID-19 observed in humans. We infected young (9-10 months) and adult (36-48 months) male ferrets with SARS-CoV-2 through either intranasal (i.n.) or intratracheal (i.t.) inoculation (**Figure 1A**). To show that adult ferrets differed from young ferrets immunologically, we performed baseline whole blood trucounts. Compared to young ferrets, B and T cell numbers were lower in adult ferrets (**Figure 1B** and **Supplemental Figure 1**), which has also been described for older humans (47). Ferrets were then inoculated with a dose of 10^7 $TCID_{50}$ as others have reported that a low dose is insufficient to establish infection (32). On 5, 14, and 21 days post infection (dpi), three animals per group were euthanized to study viral replication, pathology, and immune responses. Due to a limited supply of ferrets, no adult i.n. inoculated animals were euthanized on 14 dpi. Mock-infected young and adult ferrets inoculated i.n. with PBS were only euthanized on 14 and 21 dpi respectively.

Viral Load Is Higher After i.n. Inoculation

After i.n. SARS-CoV-2 infection, viral RNA was high in nose, throat, and rectal swabs, with no difference between ages (**Figure 2A**). In contrast, i.t. inoculation led to reduced viral loads and was clearly influenced by age as less viral RNA was measured in young animals. Viral RNA detected by RT-qPCR does not necessarily equal the presence of infectious virus, so we determined the amount of replication-competent virus in the nose and throat by $TCID_{50}$-assay. Although viral RNA could be detected by RT-qPCR as late as 21 dpi (**Figure 2A**), infectious virus was no longer detectable by 9 dpi (**Figure 2B**). I.n. infection resulted in the highest viral titer in nose and throat. Viral titers were lower for i.t. infected ferrets, especially for young ferrets where almost all samples were below the detection limit.

Next, we measured viral RNA in various tissues on 5, 14, and 21 dpi. Similar to the swabs, viral RNA was higher in almost all tissues of i.n. inoculated ferrets at 5 dpi, independent of age (**Figure 2C**). For i.n. infected ferrets, viral RNA was high in the nasal turbinates and low in the lung. Contrary to our expectations, i.t. inoculation did not lead to more viral RNA in the LRT (lungs and trachea). Viral RNA was also detected in the gut (ileum and colon) and disseminated from the initial site of infection to the olfactory bulb, cerebrum and even into the cerebellum. In these tissues, more viral RNA was detected in ferrets infected i.n. From day 5 onwards, viral RNA declined and was only sporadically detectable at 21 dpi.

To test whether the detected viral RNA was a result from an active infection at the site of sampling, we performed both a $TCID_{50}$-assay and an RT-qPCR specific for viral subgenomic mRNA. The presence of viral subgenomic mRNA is indicative of

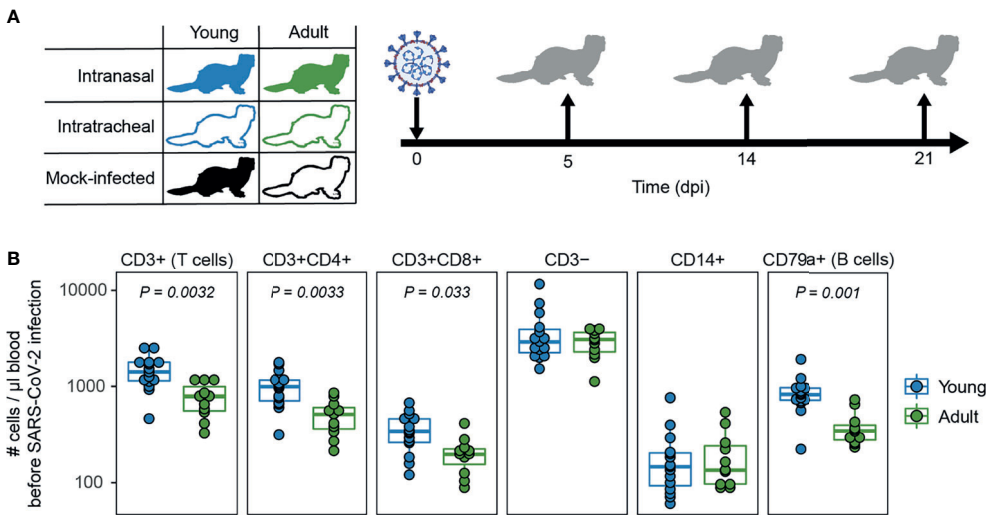

FIGURE 1 | Study outline and immunological profile of young and adult ferrets. **(A)** Young and adult ferrets were inoculated intranasally or intratracheally with 10^7 $TCID_{50}$ SARS-CoV-2 on day 0. On 5, 14 and 21 days post infection (dpi), 3 ferrets were euthanized per group. Mock-infected ferrets were euthanized on 14 dpi (young) and 21 dpi (adult). No intranasally inoculated adult ferrets were euthanized at 14 dpi due to limited availability of adult ferrets. **(B)** Cell counts in blood of uninfected young and adult ferrets. N = 15 for young animals and n = 11 for adult animals. Boxplots depict the median with the first and third quartiles. Differences between young and adult ferrets were tested *via* a two-sample Wilcoxon test and corrected for multiple testing using the Holm method. Panel **(A)** was created using BioRender.

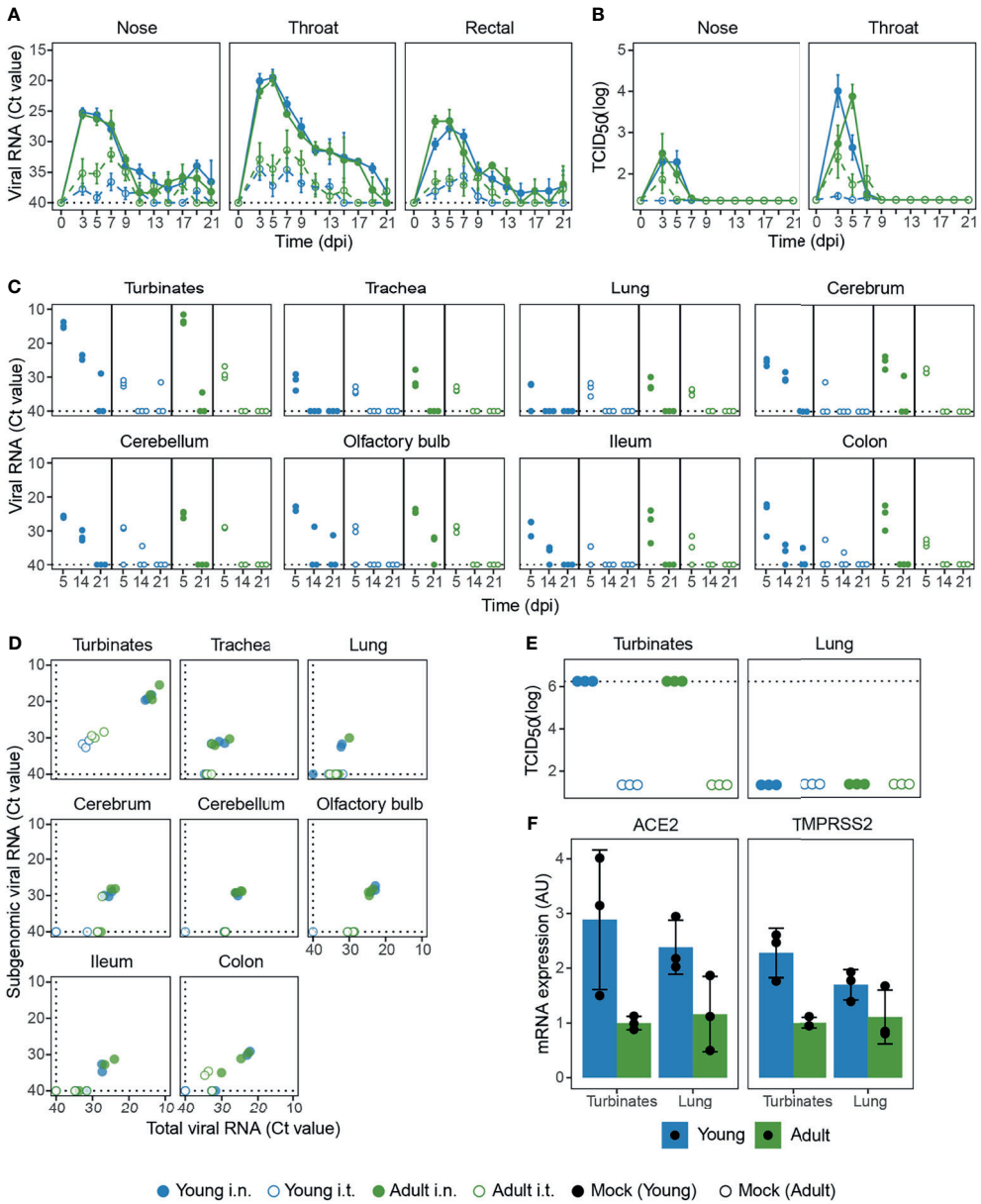

FIGURE 2 | Viral load in swabs and tissues of SARS-CoV-2 infected ferrets. **(A, B)** Viral load measured by RT-qPCR **(A)** and $TCID_{50}$-assay **(B)** in swabs collected from SARS-CoV-2 infected ferrets on various days post infection (dpi). **(C)** Viral RNA in tissues at 5, 14 and 21 dpi measured by RT-qPCR. **(D)** Total viral RNA on 5 dpi as depicted in **(C)** plotted against subgenomic viral RNA. **(E)** Infectious virus detected by $TCID_{50}$-assay in nasal turbinates and lung 5 dpi. **(F)** Expression of SARS-CoV-2 receptor ACE2 and TMPRSS2 protease in nasal turbinate and lung tissue of placebo animals, plotted as arbitrary units (AU). In panels **(A, C, D)** RT-qPCR negative specimens were set to a Ct-value of 40 for visualization purposes, which is depicted by dotted lines. In panel **(E)**, dotted lines depict the highest dilution tested. For **(A, B)** n = 3-9. For **(C, F)** with exception of 'Adult i.t.' on 14 dpi (n = 2), all groups are n = 3.

previous or current viral transcription in infected cells and was detected in most tissues 5 dpi (**Figure 2D**), but declined afterwards. By 14 dpi viral subgenomic mRNA was only detected in the nasal turbinates of young i.n. inoculated ferrets and at 21 dpi all tissues tested negative (data not shown). Interestingly, while the presence of subgenomic mRNA indicates that SARS-CoV-2 infected multiple tissues 5 dpi, this did not result in the production of detectable infectious viral particles. Analysis by $TCID_{50}$ showed that infectious virus was only produced in the nasal turbinates at 5 dpi, with no detectable infectious virus in the lung, gut or brain at 5 dpi or later timepoints (**Figure 2E** and data not shown). Due to limited tissue availability, viral $TCID_{50}$-titers in nasal turbinates were not tested on 14 and 21 dpi.

Infection of cells by SARS-CoV-2 is dependent on the expression of the binding receptor ACE2 (Angiotensin-converting enzyme 2) and the fusion priming protease

TMPRSS2 (Transmembrane protease, serine 2) (1, 48, 49). In order to determine if the reduced replication of SARS-CoV-2 in the LRT of young animals could be explained by lower ACE2 and TMPRSS2 expression, we quantified ACE2 and TMPRSS2 mRNA by RT-qPCR in young and adult placebo animals. ACE2 and TMPRSS2 expression was however similar between nasal turbinates and lung tissue, indicating that the absence of SARS-CoV-2 replication in the LRT was not due to reduced expression of ACE2 or TMPRSS2 (**Figure 2F**). Adult animals did seem to express lower levels of ACE2 and TMPRSS2, but this did not negatively impact viral load (**Figures 2A, B**).

Pathology in the URT is Higher for i.n. Infected Animals

Despite active SARS-CoV-2 replication, ferrets did not display any overt clinical signs of COVID-19 disease that are observed for humans. Compared to mock-infected animals, SARS-CoV-2-infected animals did not lose more weight and did not experience fever (**Supplemental Figures 2A, B**), nor were alterations in respiratory function and physical activity observed. Despite the absence of clinical disease, infection with SARS-CoV-2 did result in pathological aberrations in the respiratory tract as determined by histopathology.

In the nasal turbinates, pathological aberrations were restricted to the respiratory epithelial lining of the naso- and maxilloturbinates (**Figure 3A**). The sub- and intraepithelial inflammation resulted in thickened respiratory mucosa and an exudate of polymorphonuclear cells, lymphocytes and some macrophages. Damage to the epithelial lining was characterized by hypertrophy, hyperplasia, and squamous metaplasia and sporadically the epithelium was absent. Hypertrophy of goblet cells was also present and haemorrhage was sometimes observed. The different pathological facets were categorized into inflammation and damage, for which an end-score was determined as previously described (**Figures 3B, C** and **Supplemental Figure 3**) (50).

In general, the severity of pathology was dependent on age and infection route, although the age-correlation was opposite to our expectations. In the acute phase (5 dpi), i.n. inoculated ferrets displayed more pathological aberrations in the nasal turbinates, which partly resolved by 14 dpi (**Figures 3B, C**). Strikingly, inflammation and to a lesser extent epithelial damage increased again by 21 dpi in young animals, but was less pronounced in adult ferrets. Notably, this effect was stronger in i.t. infected young ferrets than in i.n. infected young ferrets and involved 100% of the epithelium of the naso- en maxilloturbinates (**Figure 3D**). Pathology in the nasal turbinates thus increased in young animals even after the infection had been cleared.

Pathology in the LRT Is Not Affected by Inoculation Route

On a macroscopic level, the lungs of SARS-CoV-2 infected ferrets did not show aberrations in the acute phase (5 dpi), apart from a few darker patches. However, red opalescent coloring along the bronchus and as isolated patches started to appear at 14 and 21 dpi. During the course of this study, there was no increase in lung weight, indicating absence of serious edema (**Supplemental Figure 2C**). Microscopically, slight peribronchi(oli)tis – characterized by the presence of

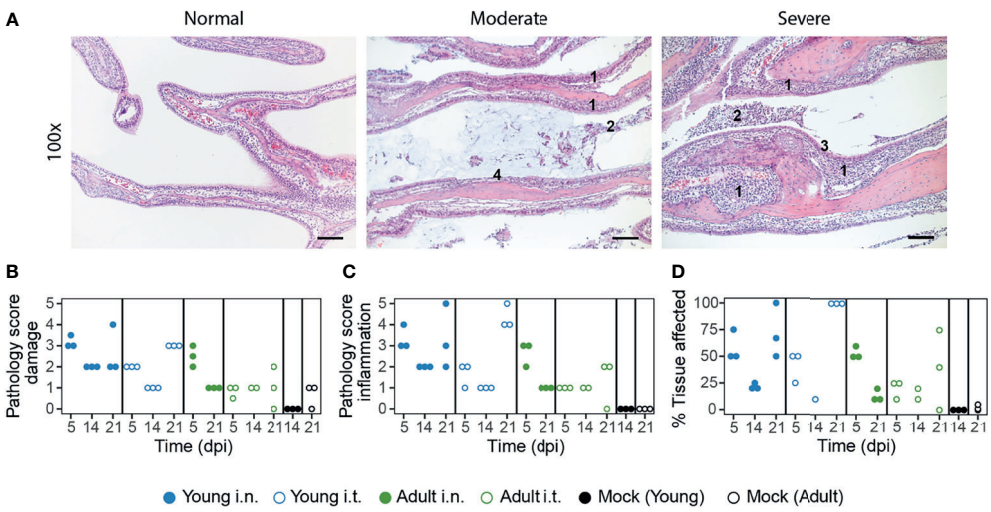

FIGURE 3 | SARS-CoV-2 infection induces more severe URT pathology in young ferrets. **(A)** Representative haematoxylin and eosin stained sections of normal, moderate (score 2) and severe (score 4) affected naso- and maxilloturbinates at 100x magnification. SARS-CoV-2 infection induced infiltration of polymorphonuclear cells into the lamina propria and submucosa of the respiratory epithelium, resulting in thickened respiratory mucosa (indicated with '1'). This was accompanied by exudate containing mucus (moderate) and many polymorphonuclear cells, lymphocytes and some macrophages (2). The infection caused hyperplasia/hypertrophy of the epithelial cells (3) and sometimes the epithelial lining was absent (4). Images are from SARS-CoV-2 infected ferrets at 5 ('moderate and severe) or 21 dpi ('normal'). Bars represent 100µm. **(B–D)** Scoring by parameters related to epithelial damage **(B)**, inflammation **(C)** and percentage of tissue involved in pathologic changes **(D)**. The infection-induced pathology was scored on a scale of 0–5 based on the parameters described in the materials and methods. With exception of 'Adult i.t.' on 14 dpi (n = 2), all groups are n = 3 and each dot represents an animal.

infiltrating cells in the sub-mucosa along the bronchi – was observed 5 dpi (**Figure 4A**). The bronchus epithelium showed some reaction in the form of mild to minor hyperplasia, sometimes visible as repeated epithelial bumps. Strikingly, hyperplasia of the Bronchus-Associated Lymphoid Tissue (BALT) developed in 1 out of 3 i.n. and in 2 out of 3 i.t. infected young ferrets by 21 dpi, but was absent in adult ferrets. Mild to strong follicular hyperplasia was located at the first branches of the bronchus and in the more severe cases extended to the smaller bronchiole (**Figure 4A**). Obstruction of bronchioli occurred regularly due to compression by the hyperplastic follicles. These consisted of activated lymphocytes, which penetrated through the muscle layer of the bronch(iol)us into the lamina propria. In addition, albeit low in number, local patches of mild to moderate desquamative interstitial pneumonia had developed. The pathology score and percentage affected lung parenchyma increased from 5 to 21 dpi, mostly in in the young ferrets (**Figures 4B, C** and **Supplemental Figure 4**). Of note, young animals that were investigated 21 dpi had tested positive for antibodies against NL-63 and enteric and systemic corona viruses prior to SARS-CoV-2 infection (**Supplemental Table 1**). This combination was absent in adult ferrets, complicating the interpretation of these results.

In concordance with our findings in the lung and nasal turbinates, pathology in the trachea increased by 21 dpi (**Figure 4D** and **Supplemental Figure 5**). The epithelium of the trachea in all young ferrets and in the i.t. adult group was often hyperplastic and sometimes showed serious damage and pseudo squamous characteristics 21 dpi (**Figure 4E**). Inflammatory cells infiltrated the submucosa and epithelium, most prominently in young ferrets. Since SARS-CoV-2 viral RNA was also detected in the gut, histopathological analysis of the ileum and colon was performed, but no deviations were observed. In conclusion, independent of inoculation route, young animals displayed more severe pathology than adult ferrets in both the URT and LRT, but it is uncertain whether the increase until 21 dpi is due to age or prior exposure to other coronaviruses.

Cellular and Humoral Immunity

As several ferrets used in this study displayed antibody responses against ferret corona viruses and NL-63 prior to the start of the study (**Supplemental Table 1**), we wondered if cross-reactive responses to SARS-CoV-2 were present in these animals. We measured antibody responses against SARS-CoV-2 spike protein (S) and its receptor binding domain (RBD) by ELISA. Cellular responses were measured by IFNγ-ELISpot in which PBMCs were stimulated with live SARS-CoV-2 or overlapping peptide pools of the S, membrane (M) and nucleoprotein (N) proteins. In three animals the antibody response against SARS-CoV-2 was just above background prior to infection (**Supplemental Figure 6A**). Additionally, another animal in the young i.n. infected group clearly responded against an overlapping peptide pool of SARS-CoV-2 spike protein in ELISpot on two separate time-points before infection (**Supplemental Figure 6B**). This animal tested positive for antibodies against ferret corona and NL63, but not against SARS-CoV-2 (**Supplemental Table 1** and **Supplemental Figure 6A**), suggesting that there might have been a cross-reactive T cell response. Interestingly, the animal displayed similar viral kinetics as other animals of the same treatment group, but it displayed more severe pathology 21 dpi.

After SARS-CoV-2 infection, i.n. inoculated ferrets displayed high antibody responses against both S and RBD with no evident differences between young and adult animals 14 dpi (**Figure 5A**). In contrast, antibody titers in i.t. infected animals were lower with a clear distinction between ages. More adult (4/5) than young (1/6) i.t. inoculated ferrets displayed responses against S-protein after infection. Similar findings were obtained for humoral responses against RBD.

Next, we investigated cellular responses at 14 dpi. PBMCs mainly responded against the larger peptide pools of S (S1 & S2), M and N (**Figure 5B**). We additionally measured responses against envelope (E) and accessory proteins (ORF3a-ORF10), but responses against these peptide pools were marginal and did not differ from naïve animals. Consistent with the low viral load, only 1/6 young i.t. infected animals responded to any SARS-CoV-2 stimulus, indicating that almost no cellular immunity was established in this group by 14 dpi. For the other groups, no clear differences between infection routes or age were observed. The responses 21 dpi were similar to those of 14 dpi (**Supplemental Figure 7A**). As others have reported the presence of cross-reactive T cell responses in humans (51–54), we also tested if PBMCs from SARS-CoV-2 infected ferrets would respond upon stimulation with spike peptide pools of coronaviruses NL63, OC43, 229E and HKU1. Some animals displayed minor responses, although they were only slightly higher than mock-infected animals (**Figure 5C**).

We additionally investigated cellular responses in the lung. To reduce contamination of the lung lymphocytes with circulating lymphocytes, lungs were perfused with saline on 14 and 21 dpi. In comparison to PBMCs, responses against the smaller SARS-CoV-2 peptide pools seemed more prominent in lung-derived lymphocytes of young i.n. infected animals. In this group, two out of three ferrets showed responses against ORF3a, ORF6, ORF8, ORF9b and ORF10 peptide pools at 21 dpi (**Figure 5D**). Like in PBMC, cellular responses were absent in the lung of i.t. infected young ferrets. Of note, responses in the lungs of i.t. infected old animals differed between day 14 and 21 post infection, with responses being higher overall on 21 dpi (**Figure 5D** and **Supplemental Figure 7B**). However, the group size (n = 2-3) was too small for reliable statistical testing.

DISCUSSION

In this study we utilized a male ferret model to assess the influence of age and infection route on SARS-CoV-2 disease and immunity. Intranasal inoculation was more efficient in establishing an infection compared to intratracheal administration. This was especially the case for young ferrets, in which virus hardly replicated after i.t.

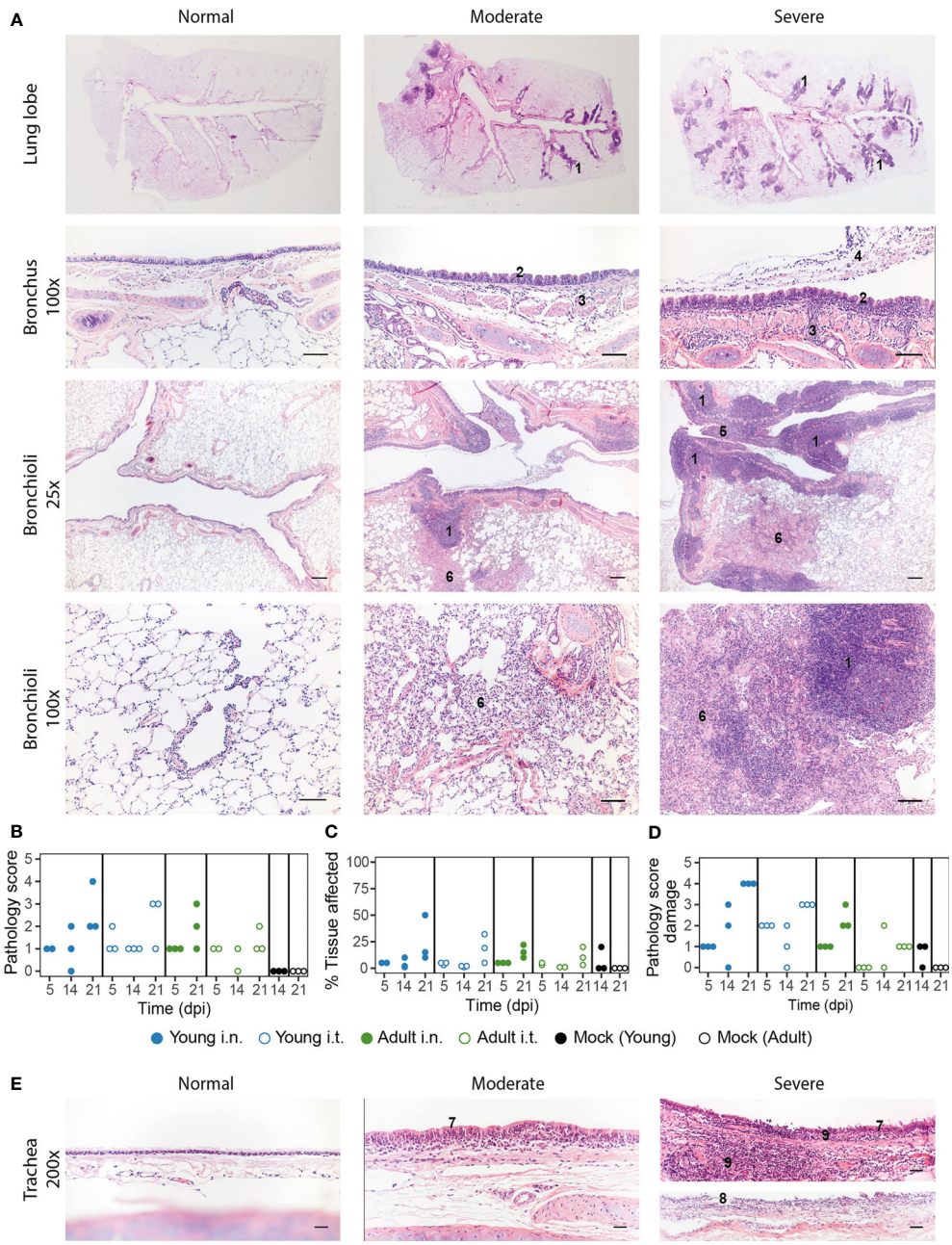

FIGURE 4 | Pathology aspects of lung and trachea. **(A)** Representative haematoxylin and eosin stained sections of normal, moderately and severely affected respiratory tissues at overview, 25x and 200x magnification. Lungs of SARS-CoV-2 infected animals with a clear hyperplasia of the Bronchus-Associated Lymphoid Tissue (BALT), consisting of activated lymphocytes that penetrate through the muscle layer of the bronch(iol)us into the lamina propria and submucosa (indicated in figure with '1'). Hyperplasia of bronchial epithelium visible as repeated bumps (2), cellular infiltrate into the submucosa (3) and exudate in the lumen (4) were also observed. The presence of hyper-plastic follicles led to obstruction of bronchiole (5). Some animals displayed desquamative interstitial pneumonia, with pulmonary macrophages in the alveoli and to a minor extent, lymphocytes and plasma cells (6). The alveolar epithelium (pneumocytes) exhibited squamous-like characteristics. Images are taken from placebo ferrets ('normal') or SARS-CoV-2 infected ferrets 14 or 21 dpi ('moderate', 'severe'). **(B-D)** Pathology was summarized in an overall score ranging from 0-5 based on the parameters described in the materials and methods. Pathology score **(B)** and % of tissue affected **(C)** for lung tissue and pathology score for trachea **(D)**. With exception of 'Adult i.t.' on 14 dpi (n = 2), all groups are n = 3. **(E)** Representative haematoxylin and eosin stained sections of normal, moderately and severely affected trachea tissue slides at 200x magnification. Pathological aberrations in the trachea consisted of hyperplasia (7), damage and pseudo-squamous characteristics of the epithelium (8) and infiltration of inflammatory cells into the submucosa and epithelium of the trachea (9). Images are taken from SARS-CoV-2 infected ferrets 5 ('normal) or 21 dpi ('moderate', 'severe').Bars represent 200µm, 100µm and 50µm at respectively 25x, 100x and 200x magnification.

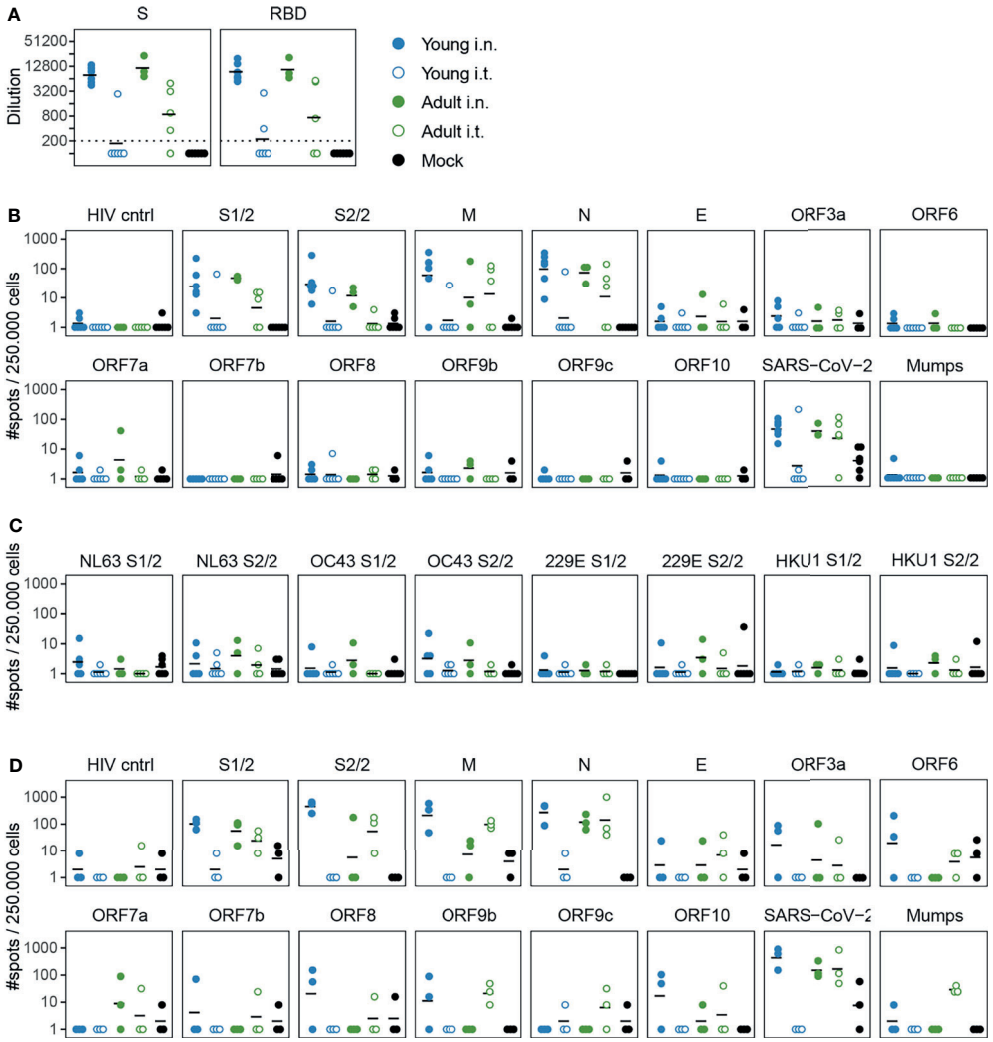

FIGURE 5 | Cellular and humoral responses in SARS-CoV-2 infected ferrets are affected by inoculation route. **(A)** Humoral responses detected by ELISA against whole spike (S) and the receptor binding domain (RBD) region of spike in serum 14 dpi. Responses are depicted as the (modelled) dilution at which the ELISA curve drops below background (mean + 3x SD of SARS-CoV-2 naïve animals at 200x dilution). The dotted line indicates the lowest dilution tested and negative samples were set to half that dilution for visualization purposes. **(B–D)** Cellular responses in PBMCs **(B, C)** and lung-derived lymphocytes **(D)** as determined by IFNγ-ELISpot. Cells were stimulated with SARS-CoV-2 peptide pools or live virus. HIV cntrl and Mumps are negative controls for peptide pool and virus stimulations respectively. Data shown here were corrected for medium background and were set to a minimum of 1 spot for visualization on a log-scale. **(B)** PBMCs isolated 14 or 15 days post infection (dpi). **(C)** Frozen PBMCs isolated 14 or 21 dpi were thawed and stimulated with peptide pools of endemic human coronaviruses. **(D)** Responses by lung-derived lymphocytes at 21 dpi. For b and c, samples were collected 14 and 15 or 14 and 21 dpi respectively, but visualized as a single group. N = 3-6 for panels **(A–C)** and n = 3 for panel **(D)**. Black lines indicate (geometric) mean per group.

inoculation. In contrast, disease and pathology were not increased in older animals or upon intratracheal inoculation.

Despite a productive SARS-CoV-2 infection, ferrets did not develop the symptomatic disease that is reported for humans (reviewed in (16)). A slightly more watery defecation was observed in some animals towards the end of the study, but occurrences were too few to confidently attribute this to SARS-CoV-2 infection. We did however detect SARS-CoV-2 genomic RNA and subgenomic mRNA in rectal swabs and gut tissues at multiple time-points. Subgenomic SARS-CoV-2 mRNA is indicative of viral infection, which suggests that SARS-CoV-2 is indeed enterotropic in ferrets, similar to what has been reported for humans (14, 55–58). In addition, the presence of viral genomic RNA and subgenomic mRNA in the olfactory bulb, cerebrum and cerebellum of ferrets is in line with reports that SARS-CoV-2 can infect the CNS of patients (14, 59, 60). Infection of the olfactory bulb might explain the anosmia often found in COVID-19 patients. It is however important to note that while the presence of subgenomic mRNA indicates infection of various tissues, there was a lack of infectious virus as measured by $TCID_{50}$-assay. This

raises the question whether the production of infectious virus in these tissues is completely absent or only happened within the first few days after inoculation.

The lack of clinical disease in this study is in line with previous SARS-CoV-2 ferret studies. In those studies bodyweight did not decrease after infection, although reduced activity was observed in some instances (25, 29, 32). Fever was observed in some studies (25, 27), but not in others (29, 32, 33). Ferrets thus do not model the severe aspects of COVID-19. Despite this knowledge, we initiated this study because existing studies did not investigate intratracheal inoculation in (older) male ferrets. Shi et al. did perform an intratracheal infection in female ferrets and found viral RNA in the nasal turbinates and trachea, but not in the lung (30). In our study, adult male ferrets displayed higher viral titers after i.t. infection compared to young ferrets, indicating that age increases susceptibility to LRT SARS-CoV-2 infection in the ferret model. We postulated that the reduced viral replication in the LRT of especially young ferrets might be due to differential expression of the SARS-CoV-2 receptors ACE2 and TMPRSS2 (1, 49). However, this does not seem to be the case as ACE2 and TMPRSS2 expression was similar between nasal turbinate and lung tissue and young ferrets actually expressed more ACE2 and TMRPSS2 than adult ferrets. It thus seems that factors other than receptor expression prevent the successful replication of SARS-CoV-2 in the LRT of young ferrets. Other age-dependent factors that are thought to affect SARS-CoV-2 replication include the immune system, the presence of comorbidities and the status of the vascular endothelium (61). Further research might clarify to which extent these variables influence the ferret response to SARS-CoV-2 infection.

Notwithstanding the lack of clinical symptoms, we and others (30, 32) did find pathological abnormalities in infected ferrets. While SARS-CoV-2 replicated less efficiently in young i.t. inoculated animals and almost no adaptive immune response was induced, they did display some of the most affected pathology. It is however important to mention that all young ferrets euthanized on 21 dpi tested positive for antibodies against ferret corona and NL63 prior to SARS-CoV-2 infection. We cannot exclude that this might have had an effect and it has been postulated that existing cross-reactive immune responses can worsen COVID-19 disease outcome (62). Ryan et al. also found that pathology was still increasing between 14 and 21 dpi, although they did not report the immune status of their ferrets for other corona viruses. It is tempting to speculate that the increasing pathology post SARS-CoV-2 infection partly resembles aspects of long-COVID that have been described in convalescent patients (22, 63–65). These patients suffer from sequala up to months after initial infection with SARS-CoV-2. Although the symptoms are diverse, dyspnea is a relatively common occurrence. In theory, the BALT hyperplasia that we observed in ferrets and the resulting constriction of the bronchi(oli) could induce dyspnea, although there is no evidence yet that this is the cause of dyspnea in patients suffering from long-COVID.

After SARS-CoV-2 infection we detected antibodies against SARS-CoV-2 S-protein and RBD. Antibody titers were highest in i.n. infected ferrets, low in adult i.t. infected animals and absent in most young i.t. infected animals. This suggest that sufficient viral replication is required for seroconversion, as ferrets with lower viral loads also displayed lower humoral responses. This was especially clear in the i.t. young group, where the only ferret that developed humoral and cellular immunity also possessed the highest titer of replicative competent virus. Cellular responses were also strongest in i.n. inoculated ferrets. Similar to cellular responses of convalescent patients (54, 66), most responses in ferrets were aimed against S, M and N proteins. In both ferrets and humans (54, 66), almost no response against the E protein was observed. Cellular responses against multiple accessory proteins of SARS-CoV-2 were limited in the blood, but lung-derived lymphocytes did respond against several of these peptide pools. Likely, the relative abundance of SARS-CoV-2 specific T cells is higher in the lung, thereby increasing the sensitivity of the ELISpot assay. As cross-reactive cellular responses for SARS-CoV-2 have been described in humans (51–54), we also measured responses in the blood against peptide pools of S-proteins of other corona viruses. However, responses were low and interpretation of the results will require a larger group size and more sensitive assays.

Due to the global circumstances at the time of this study, there are several caveats present in the experimental set-up. The availability of (male) ferrets was limited and hence we could not investigate all groups at every timepoint. In addition, several ferrets were previously exposed to Aleutian disease and coronaviruses other than SARS-CoV-2 (details in Supplemental data). Although we did not find evidence that this infection history influenced our results, we cannot fully exclude that possibility. Finally, due to the limited availability of animals it will be difficult to model SARS-CoV-2 infections in older ferrets. However, as we did not find strong differences between young and adult ferrets upon intranasal inoculation, the use of young ferrets should suffice for future experiments.

As has been discussed here, ferrets are readily infected with SARS-CoV-2 but do not present clinical symptoms. Infected ferrets might thus represent the asymptomatic COVID-19 that manifests in a significant part of the population (67). In addition, the derailed immune responses in the respiratory tract in ferrets might model the long-term respiratory effects observed in long-COVID patients, although more in-depth research is required to verify this. Lastly, with the recently developed reagents for humoral and cellular immunology in the ferret model (37, 68–71), vaccine-induced immune responses can be quantified and their effect on viral replication and pathology can be measured. This matured ferret model can help with improving our understanding of SARS-CoV-2, thereby driving the development of new therapies and vaccines.

DATA AVAILABILITY STATEMENT

All raw data files are being stored in-house on backed-up servers and are available upon reasonable request to the corresponding author. The sequence of the SARS-CoV-2 isolate can be found on

GISAID (accession ID: EPI_ISL_454753). Correspondence and requests for materials should be addressed to JdJ.

ETHICS STATEMENT

The animal study was reviewed and approved by the Animal Welfare Body of the Antonie van Leeuwenhoek terrain.

AUTHOR CONTRIBUTIONS

Conceptualization: KV and JJ. Methodology: KV and JJ. Investigation: KV, HD, LW, AG, TS, JK, and SL. Formal analysis: KV, PR, PK, and JJ. Visualization: KV. Supervision: JJ and PK. Writing—original draft: KV, JJ, and PK. Writing—review & editing: KV, JJ, PK, AM, and PR. All authors contributed to the article and approved the submitted version.

FUNDING

This work was funded by the Dutch Ministry of Health, Welfare, and Sports (VWS).

ACKNOWLEDGMENTS

We would like to thank Gabriel Goderski for isolating and growing the initial SARS-CoV-2 isolate and Jeroen Cremer for sequencing. We are also grateful to Josien Lanfermeijer with help during animal sections, the biotechnicians from the animal facility for excellent care-taking of the animals and Dr. Willem Luytjes for critical reviewing of the manuscript.

SUPPLEMENTARY MATERIAL

The Supplementary Material for this article can be found online at: https://www.frontiersin.org/articles/10.3389/fimmu.2021.750229/full#supplementary-material

REFERENCES

1. Zhou P, Yang XL, Wang XG, Hu B, Zhang L, Zhang W, et al. A Pneumonia Outbreak Associated With a New Coronavirus of Probable Bat Origin. *Nature* (2020) 579(7798):270–3. doi: 10.1038/s41586-020-2012-7
2. Creech CB, Walker SC, Samuels RJ. SARS-CoV-2 Vaccines. *JAMA* (2021) 325 (13):1318–20. doi: 10.1001/jama.2021.3199
3. Gupta RK. Will SARS-CoV-2 Variants of Concern Affect the Promise of Vaccines? *Nat Rev Immunol* (2021) 21(6):340–1. doi: 10.1038/s41577-021-00556-5
4. Munoz-Fontela C, Dowling WE, Funnell SGP, Gsell PS, Riveros-Balta AX, Albrecht RA, et al. Animal Models for COVID-19. *Nature* (2020) 586 (7830):509–15. doi: 10.1038/s41586-020-2787-6
5. Lee CY, Lowen AC. Animal Models for SARS-CoV-2. *Curr Opin Virol* (2021) 48:73–81. doi: 10.1016/j.coviro.2021.03.009
6. WHO. *Transmission of SARS-CoV-2: Implications for Infection Prevention Precautions*. WHO (2020).
7. Harrison AG, Lin T, Wang P. Mechanisms of SARS-CoV-2 Transmission and Pathogenesis. *Trends Immunol* (2020) 41(12):1100–15. doi: 10.1016/j.it.2020.10.004
8. Tang S, Mao Y, Jones RM, Tan Q, Ji JS, Li N, et al. Aerosol Transmission of SARS-CoV-2? Evidence, Prevention and Control. *Environ Int* (2020) 144:106039. doi: 10.1016/j.envint.2020.106039
9. Liu Y, Ning Z, Chen Y, Guo M, Liu Y, Gali NK, et al. Aerodynamic Analysis of SARS-CoV-2 in Two Wuhan Hospitals. *Nature* (2020) 582(7813):557–60. doi: 10.1038/s41586-020-2271-3
10. Chen Y, Chen L, Deng Q, Zhang G, Wu K, Ni L, et al. The Presence of SARS-CoV-2 RNA in the Feces of COVID-19 Patients. *J Med Virol* (2020) 92 (7):833–40. doi: 10.1002/jmv.25825
11. Zheng S, Fan J, Yu F, Feng B, Lou B, Zou Q, et al. Viral Load Dynamics and Disease Severity in Patients Infected With SARS-CoV-2 in Zhejiang Province, China, January-March 2020: Retrospective Cohort Study. *BMJ* (2020) 369: m1443. doi: 10.1136/bmj.m1443
12. Wolfel R, Corman VM, Guggemos W, Seilmaier M, Zange S, Muller MA, et al. Virological Assessment of Hospitalized Patients With COVID-2019. *Nature* (2020) 581(7809):465–9. doi: 10.1038/s41586-020-2196-x
13. Amirian ES. Potential Fecal Transmission of SARS-CoV-2: Current Evidence and Implications for Public Health. *Int J Infect Dis* (2020) 95:363–70. doi: 10.1016/j.ijid.2020.04.057
14. Schurink B, Roos E, Radonic T, Barbe E, Bouman CSC, de Boer HH, et al. Viral Presence and Immunopathology in Patients With Lethal COVID-19: A Prospective Autopsy Cohort Study. *Lancet Microbe* (2020) 1(7):e290–9. doi: 10.1016/s2666-5247(20)30144-0
15. Zhou F, Yu T, Du R, Fan G, Liu Y, Liu Z, et al. Clinical Course and Risk Factors for Mortality of Adult Inpatients With COVID-19 in Wuhan, China: A Retrospective Cohort Study. *Lancet* (2020) 395(10229):1054–62. doi: 10.1016/s0140-6736(20)30566-3
16. Ge H, Wang X, Yuan X, Xiao G, Wang C, Deng T, et al. The Epidemiology and Clinical Information About COVID-19. *Eur J Clin Microbiol Infect Dis* (2020) 39(6):1011–9. doi: 10.1007/s10096-020-03874-z
17. Du Y, Tu L, Zhu P, Mu M, Wang R, Yang P, et al. Clinical Features of 85 Fatal Cases of COVID-19 From Wuhan. A Retrospective Observational Study. *Am J Respir Crit Care Med* (2020) 201(11):1372–9. doi: 10.1164/rccm.202003-0543OC
18. Bradley BT, Maioli H, Johnston R, Chaudhry I, Fink SL, Xu H, et al. Histopathology and Ultrastructural Findings of Fatal COVID-19 Infections in Washington State: A Case Series. *Lancet* (2020) 396(10247):320–32. doi: 10.1016/s0140-6736(20)31305-2
19. Cdc Weekly C. The Epidemiological Characteristics of an Outbreak of 2019 Novel Coronavirus Diseases (COVID-19) — China, 2020. *China CDC Weekly* (2020) 2(8):113–22. doi: 10.46234/ccdcw2020.032
20. Karagiannidis C, Mostert C, Hentschker C, Voshaar T, Malzahn J, Schillinger G, et al. Case Characteristics, Resource Use, and Outcomes of 10 021 Patients With COVID-19 Admitted to 920 German Hospitals: An Observational Study. *Lancet Respir Med* (2020) 8(9):853–62. doi: 10.1016/s2213-2600(20)30316-7
21. Verity R, Okell LC, Dorigatti I, Winskill P, Whittaker C, Imai N, et al. Estimates of the Severity of Coronavirus Disease 2019: A Model-Based Analysis. *Lancet Infect Dis* (2020) 20(6):669–77. doi: 10.1016/s1473-3099(20)30243-7
22. Nalbandian A, Sehgal K, Gupta A, Madhavan MV, McGroder C, Stevens JS, et al. Post-Acute COVID-19 Syndrome. *Nat Med* (2021) 27(4):601–15. doi: 10.1038/s41591-021-01283-z
23. Belser JA, Katz JM, Tumpey TM. The Ferret as a Model Organism to Study Influenza A Virus Infection. *Dis Models Mech* (2011) 4:575–9. doi: 10.1242/dmm.007823
24. Bodewes R, Rimmelzwaan GF, Osterhaus AD. Animal Models for the Preclinical Evaluation of Candidate Influenza Vaccines. *Expert Rev Vaccines* (2010) 9(1):59–72. doi: 10.1586/erv.09.148
25. Kim YI, Kim SG, Kim SM, Kim EH, Park SJ, Yu KM, et al. Infection and Rapid Transmission of SARS-CoV-2 in Ferrets. *Cell Host Microbe* (2020) 27(5):704–9.e2. doi: 10.1016/j.chom.2020.03.023
26. Liu HL, Yeh IJ, Phan NN, Wu YH, Yen MC, Hung JH, et al. Gene Signatures of SARS-CoV/SARS-CoV-2-Infected Ferret Lungs in Short- and Long-Term Models. *Infect Genet Evol* (2020) 85:104438. doi: 10.1016/j.meegid.2020.104438

27. Park SJ, Yu KM, Kim YI, Kim SM, Kim EH, Kim SG, et al. Antiviral Efficacies of FDA-Approved Drugs Against SARS-CoV-2 Infection in Ferrets. *mBio* (2020) 11(3):e01114–20. doi: 10.1128/mBio.01114-20
28. Richard M, Kok A, de Meulder D, Bestebroer TM, Lamers MM, Okba NMA, et al. SARS-CoV-2 is Transmitted *via* Contact and *via* the Air Between Ferrets. *Nat Commun* (2020) 11(1):3496. doi: 10.1038/s41467-020-17367-2
29. Schlottau K, Rissmann M, Graaf A, Schön J, Sehl J, Wylezich C, et al. SARS-CoV-2 in Fruit Bats, Ferrets, Pigs, and Chickens: An Experimental Transmission Study. *Lancet Microbe* (2020) 1(5):e218–25. doi: 10.1016/s2666-5247(20)30089-6
30. Shi J, Wen Z, Zhong G, Yang H, Wang C, Huang B, et al. Susceptibility of Ferrets, Cats, Dogs, and Other Domesticated Animals to SARS-Coronavirus 2. *Science* (2020) 368(6494):1016–20. doi: 10.1126/science.abb7015
31. Wu S, Zhong G, Zhang J, Shuai L, Zhang Z, Wen Z, et al. A Single Dose of an Adenovirus-Vectored Vaccine Provides Protection Against SARS-CoV-2 Challenge. *Nat Commun* (2020) 11(1):4081. doi: 10.1038/s41467-020-17972-1
32. Ryan KA, Bewley KR, Fotheringham SA, Slack GS, Brown P, Hall Y, et al. Dose-Dependent Response to Infection With SARS-CoV-2 in the Ferret Model and Evidence of Protective Immunity. *Nat Commun* (2021) 12(1):81. doi: 10.1038/s41467-020-20439-y
33. Everett HE, Lean FZX, Byrne AMP, van Diemen PM, Rhodes S, James J, et al. Intranasal Infection of Ferrets With SARS-CoV-2 as a Model for Asymptomatic Human Infection. *Viruses* (2021) 13(1):113. doi: 10.3390/v13010113
34. Kreijtz JH, Kroeze EJ, Stittelaar KJ, de Waal L, van Amerongen G, van Trierum S, et al. Low Pathogenic Avian Influenza A(H7N9) Virus Causes High Mortality in Ferrets Upon Intratracheal Challenge: A Model to Study Intervention Strategies. *Vaccine* (2013) 31(43):4995–9. doi: 10.1016/j.vaccine.2013.06.071
35. de Jonge J, Isakova-Sivak I, van Dijken H, Spijkers S, Mouthaan J, de Jong R, et al. H7N9 Live Attenuated Influenza Vaccine is Highly Immunogenic, Prevents Virus Replication and Protects Against Severe Bronchopneumonia in Ferrets. *Mol Ther* (2016) 24:1–12. doi: 10.1038/mt.2016.23
36. Bodewes R, Kreijtz JHCM, Van Amerongen G, Fouchier RAM, Osterhaus ADME, Rimmelzwaan GF, et al. Pathogenesis of Influenza A/H5N1 Virus Infection in Ferrets Differs Between Intranasal and Intratracheal Routes of Inoculation. *Am J Pathol* (2011) 179:30–6. doi: 10.1016/j.ajpath.2011.03.026
37. van de Ven K, de Heij F, van Dijken H, Ferreira JA, de Jonge J. Systemic and Respiratory T-Cells Induced by Seasonal H1N1 Influenza Protect Against Pandemic H2N2 in Ferrets. *Commun Biol* (2020) 3(1):564. doi: 10.1038/s42003-020-01278-5
38. Fang Y, Rowe T, Leon AJ, Banner D, Danesh A, Xu L, et al. Molecular Characterization of *In Vivo* Adjuvant Activity in Ferrets Vaccinated Against Influenza Virus. *J Virol* (2010) 84(17):8369–88. doi: 10.1128/JVI.02305-09
39. Corman VM, Landt O, Kaiser M, Molenkamp R, Meijer A, Chu DK, et al. Detection of 2019 Novel Coronavirus (2019-Ncov) by Real-Time RT-PCR. *Euro Surveill* (2020) 25(3):2000045. doi: 10.2807/1560-7917.ES.2020.25.3.2000045
40. Scheltinga SA, Templeton KE, Beersma MF, Claas EC. Diagnosis of Human Metapneumovirus and Rhinovirus in Patients With Respiratory Tract Infections by an Internally Controlled Multiplex Real-Time RNA PCR. *J Clin Virol* (2005) 33(4):306–11. doi: 10.1016/j.jcv.2004.08.021
41. Zhang Y, Huang K, Xie D, Lau JY, Shen W, Li P, et al. *In Vivo* Structure and SARS-CoV-2 RNA Genome. *Nat Commun* (2021) 12(1):5695. doi: 1038/s41467-021-25999-1
42. R Core Team. *R: A Language and Environment for Statistical Computing. R Foundation for Statistical Computing*. (2020).
43. Wickham H. *Ggplot2: Elegant Graphics for Data Analysis*. New York: Springer-Verlag (2016).
44. Wickham H, Averick M, Bryan J, Chang W, McGowan L, François R, et al. Welcome to the Tidyverse. *J Open Source Software* (2019) 4(43):1686. doi: 10.21105/joss.01686
45. Kassambara A. *Ggpubr: 'Ggplot2' Based Publication Ready Plots CRAN*. (2020).
46. Holm S. A Simple Sequentially Rejective Multiple Test Procedure. *Scandinavian J Stat* (1979) 6(2):65–70.
47. Sansoni P, Cossarizza A, Brianti V, Fagnoni F, Snelli G, Monti D, et al. Lymphocyte Subsets and Natural Killer Cell Activity in Healthy Old People and Centenarians. *Blood* (1993) 82(9):2767–73. doi: 10.1182/blood.V82.9.2767.2767
48. Peacock TP, Goldhill DH, Zhou J, Baillon L, Frise R, Swann OC, et al. The Furin Cleavage Site in the SARS-CoV-2 Spike Protein is Required for Transmission in Ferrets. *Nat Microbiol* (2021) 6(7):899–909. doi: 10.1038/s41564-021-00908-w
49. Hoffmann M, Kleine-Weber H, Schroeder S, Kruger N, Herrler T, Erichsen S, et al. SARS-CoV-2 Cell Entry Depends on ACE2 and TMPRSS2 and Is Blocked by a Clinically Proven Protease Inhibitor. *Cell* (2020) 181(2):271–80.e8. doi: 10.1016/j.cell.2020.02.052
50. Isakova-Sivak I, de Jonge J, Smolonogina T, Rekstin A, van Amerongen G, van Dijken H, et al. Development and Pre-Clinical Evaluation of Two LAIV Strains Against Potentially Pandemic H2N2 Influenza Virus. *PLoS One* (2014) 9(7):e102339. doi: 10.1371/journal.pone.0102339
51. Braun J, Loyal L, Frentsch M, Wendisch D, Georg P, Kurth F, et al. SARS-CoV-2-Reactive T Cells in Healthy Donors and Patients With COVID-19. *Nature* (2020) 587(7833):270–4. doi: 10.1038/s41586-020-2598-9
52. Mateus J, Grifoni A, Tarke A, Sidney J, Ramirez SI, Dan JM, et al. Selective and Cross-Reactive SARS-CoV-2 T Cell Epitopes in Unexposed Humans. *Science* (2020) 370(6512):89–94. doi: 10.1126/science.abd3871
53. Le Bert N, Tan AT, Kunasegaran K, Tham CYL, Hafezi M, Chia A, et al. SARS-CoV-2-Specific T Cell Immunity in Cases of COVID-19 and SARS, and Uninfected Controls. *Nature* (2020) 584(7821):457–62. doi: 10.1038/s41586-020-2550-z
54. Grifoni A, Weiskopf D, Ramirez SI, Mateus J, Dan JM, Moderbacher CR, et al. Targets of T Cell Responses to SARS-CoV-2 Coronavirus in Humans With COVID-19 Disease and Unexposed Individuals. *Cell* (2020) 181(7):1489–501.e15. doi: 10.1016/j.cell.2020.05.015
55. Hanley B, Naresh KN, Roufosse C, Nicholson AG, Weir J, Cooke GS, et al. Histopathological Findings and Viral Tropism in UK Patients With Severe Fatal COVID-19: A Post-Mortem Study. *Lancet Microbe* (2020) 1(6):e245–53. doi: 10.1016/s2666-5247(20)30115-4
56. Lamers MM, Beumer J, van der Vaart J, Knoops K, Puschhof J, Breugem TI, et al. SARS-CoV-2 Productively Infects Human Gut Enterocytes. *Science* (2020) 369(6499):50–4. doi: 10.1126/science.abc1669
57. Cuicchi D, Lazzarotto T, Poggioli G. Fecal-Oral Transmission of SARS-CoV-2: Review of Laboratory-Confirmed Virus in Gastrointestinal System. *Int J Colorectal Dis* (2020) 36(3):437–44. doi: 10.1007/s00384-020-03785-7
58. Cheung KS, Hung IFN, Chan PPY, Lung KC, Tso E, Liu R, et al. Gastrointestinal Manifestations of SARS-CoV-2 Infection and Virus Load in Fecal Samples From a Hong Kong Cohort: Systematic Review and Meta-Analysis. *Gastroenterology* (2020) 159(1):81–95. doi: 10.1053/j.gastro.2020.03.065
59. Song E, Zhang C, Israelow B, Lu-Culligan A, Prado AV, Skriabine S, et al. Neuroinvasion of SARS-CoV-2 in Human and Mouse Brain. *J Exp Med* (2021) 218(3):e20202135. doi: 10.1084/jem.20202135
60. Meinhardt J, Radke J, Dittmayer C, Franz J, Thomas C, Mothes R, et al. Olfactory Transmucosal SARS-CoV-2 Invasion as a Port of Central Nervous System Entry in Individuals With COVID-19. *Nat Neurosci* (2021) 24(2):168–75. doi: 10.1038/s41593-020-00758-5
61. Zimmermann P, Curtis N. Why is COVID-19 Less Severe in Children? A Review of the Proposed Mechanisms Underlying the Age-Related Difference in Severity of SARS-CoV-2 Infections. *Arch Dis Child* (2020) 106:429–39. doi: 10.1136/archdischild-2020-320338
62. Beretta A, Cranage M, Zipeto D. Is Cross-Reactive Immunity Triggering COVID-19 Immunopathogenesis? *Front Immunol* (2020) 11:567710. doi: 10.3389/fimmu.2020.567710
63. Zhao YM, Shang YM, Song WB, Li QQ, Xie H, Xu QF, et al. Follow-Up Study of the Pulmonary Function and Related Physiological Characteristics of COVID-19 Survivors Three Months After Recovery. *EClinicalMedicine* (2020) 25:100463. doi: 10.1016/j.eclinm.2020.100463
64. Dennis A, Wamil M, Alberts J, Oben J, Cuthbertson DJ, Wootton D, et al. Multiorgan Impairment in Low-Risk Individuals With Post-COVID-19 Syndrome: A Prospective, Community-Based Study. *BMJ Open* (2021) 11(3):e048391. doi: 10.1136/bmjopen-2020-048391

65. Ayoubkhani D, Khunti K, Nafilyan V, Maddox T, Humberstone B, Diamond I, et al. Post-Covid Syndrome in Individuals Admitted to Hospital With Covid-19: Retrospective Cohort Study. *BMJ* (2021) 372:n693. doi: 10.1136/bmj.n693
66. Peng Y, Mentzer AJ, Liu G, Yao X, Yin Z, Dong D, et al. Broad and Strong Memory CD4+ and CD8+ T Cells Induced by SARS-CoV-2 in UK Convalescent Individuals Following COVID-19. *Nat Immunol* (2020) 21 (11):1336–45. doi: 10.1038/s41590-020-0782-6
67. Gao Z, Xu Y, Sun C, Wang X, Guo Y, Qiu S, et al. A Systematic Review of Asymptomatic Infections With COVID-19. *J Microbiol Immunol Infect* (2021) 54(1):12–6. doi: 10.1016/j.jmii.2020.05.001
68. DiPiazza A, Richards K, Batarse F, Lockard L, Zeng H, García-Sastre A, et al. Flow Cytometric and Cytokine ELISpot Approaches To Characterize the Cell-Mediated Immune Response in Ferrets Following Influenza Virus Infection. *J Virol* (2016) 90:7991–8004. doi: 10.1128/JVI.01001-16
69. Music N, Reber AJ, Lipatov AS, Kamal RP, Blanchfield K, Wilson JR, et al. Influenza Vaccination Accelerates Recovery of Ferrets From Lymphopenia. *PLoS One* (2014) 9:e100926. doi: 10.1371/journal.pone.0100926
70. DiPiazza AT, Richards KA, Liu W-C, Albrecht RA, Sant AJ. Analyses of Cellular Immune Responses in Ferrets Following Influenza Virus Infection. *Methods Mol Biol (Clifton N.J.)* (2018) 1836:513–30. doi: 10.1007/978-1-4939-8678-1_24
71. Martel CJ-M, Aasted B. Characterization of Antibodies Against Ferret Immunoglobulins, Cytokines and CD Markers. *Veterinary Immunol Immunopathol* (2009) 132:109–15. doi: 10.1016/j.vetimm.2009.05.011

Conflict of Interest: The authors declare that the research was conducted in the absence of any commercial or financial relationships that could be construed as a potential conflict of interest.